Traveling strings of active dipolar colloids

Chao, X.; Skipper, K.; Rouall, C.P.; Henkes, S.E.; Liverpool, T.B.

Traveling Strings of Active Dipolar Colloids

Xichen Chao,[1] Katherine Skipper,[2] C. Patrick Royall,[2,3] Silke Henkes,[1,4] and Tanniemola B. Liverpool[1]
[1]School of Mathematics, University of Bristol, Fry Building, Bristol BS8 1UG, United Kingdom
[2]H.H. Wills Physics Laboratory, Tyndall Avenue, Bristol BS8 1TL, United Kingdom
[3]Gulliver UMR CNRS 7083, ESPCI Paris, Université PSL, 75005 Paris, France
[4]Lorentz Institute, LION, Leiden University–Leiden 2333 CA, Netherlands

(Received 18 April 2024; revised 13 September 2024; accepted 2 December 2024; published 6 January 2025)

We study an intriguing new type of self-assembled active colloidal polymer system in 3D. It is obtained from a suspension of Janus particles in an electric field that induces parallel dipoles in the particles as well as self-propulsion in the plane perpendicular to the field. At low volume fractions, in experiment, the particles self-assemble into 3D columns that are self-propelled in 2D. Explicit numerical simulations combining dipolar interactions and active self-propulsion find an activity dependent transition to a string phase by increasing dipole strength. We classify the collective dynamics of strings as a function of rotational and translational diffusion. Using an anisotropic version of the Rouse model of polymers with active driving, we analytically compute the strings' collective dynamics and center of mass motion, which matches simulations and is consistent with experimental data. We also discover long range correlations of the fluctuations along the string contour that grow with the active persistence time, a purely active effect that disappears in the thermal limit.

DOI: 10.1103/PhysRevLett.134.018302

Active matter describes a new class of materials that are composed of elements driven out of equilibrium by internal sources of energy. They promise a novel route to functionality in materials design for numerous applications, from drug delivery to metamaterials [1–7]. A major challenge, however, is *controlling* activity, and using it to steer emergent collective behavior toward a desired function. One way to control it is by tuning the interplay between active driving and passive mechanics at scales intermediate between microscopic building blocks and macroscopic scales [8]. These dynamic mesoscale structures can be polymers [9–12], membranes [13], and disordered or ordered solids [14–17]. Their complex internal dynamics requires more detailed descriptions, going beyond long wavelength hydrodynamics, to uncover the physical principles required to accurately control them.

One-dimensional polymers are promising as their open structure leaves them more susceptible to external controls. Hence, there has been a resurgence of experimental and theoretical work on active polymer systems [18–21]. Most experimental realizations of active polymer systems have been biological, e.g., motor-driven cytoskeletal polymers [22] or living organisms such as worms [19]. Theoretical studies have included tangentially driven linear polymers and ring polymers, mostly in 2D [20,23–25] and more recently have begun to look at entanglement [26]. Biological components, however, are hard to control and there is a need for systems built from man-made (synthetic) components.

Active Janus colloids are one of the simplest experimental building blocks of synthetic active materials, their single particle dynamics well approximated by active Brownian particles [27–29]. Here, we use metallodielectric Janus particles, which, when in an oscillating electric field, due to induced-charge electrophoresis (ICEP) [30,31], simultaneously become active and interact via pairwise dipolar interactions. The colloids sediment to the bottom of the sample where they can self-assemble into 2D polymer-like motile chains [32–34]. Recent experiments have shown, however, that it is possible to study this system in 3D by using smaller Janus particles, which due to their size sediment markedly less [35]. At low volume fractions, the particles self-assemble into active columns (strings) that self-propel in the plane perpendicular to their axis. We note it is well known from experiments [36,37] and simulations [38] that passive dipolar colloids exhibit a passive string fluid phase at low volume fraction.

In this Letter, we study the collective dynamics of the low density phase of actively traveling strings through a combination of experiment, computer simulation, and analytical theory. We carry out experiments with metallosilica Janus particles which we study with confocal microscopy at the single-particle level [39]. Our numerical model combines short range repulsion, dipolar interactions

in the direction of the field and self propulsion, and we find an activity-dependent transition to the active string phase as a function of dipole strength. We explore the collective dynamics of strings as a function of rotational and translational diffusion strengths. Using a generalized Rouse model of anistropic three-dimensional flexible polymers with active driving allows us to capture the string dynamics. In addition to explaining the global string dynamics, this predicts a purely active emergent correlation length along the strings. We verify that our theoretical model agrees very well with simulations and is consistent with experiments.

Experiment—We use the 3D ICEP system [35]. A suspension of metallodielectric Janus particles of diameter $\sigma_0 = 1.5$ μm in milli-Q water and dimeythl siloxane at volume ratio 7:10 is placed in an oscillating electric field E. This solvent matches the refractive index of the particles, but not the density. The gravitational length of passive particles in the absence of the electric field is $\approx 0.15\sigma_0$. Because of the electric field induced activity, this rises to $\approx 2\sigma_0$. We study a fixed volume fraction $\phi = 0.05$. In this system, the Janus colloids move like active Brownian particles (ABPs) in a plane orthogonal to the field (xy) and diffuse in the third dimension (z) [Figs. 1(a) and 1(b)]. Because of the imbalance of the dielectric constant between the solvent and the particles, dipolar interactions are induced by the external electric field, which point in the direction of the field. For our parameters (5 kHz and NaCl at a concentration of 0.1 mM), the interactions between the particles can be approximated as a single effective dipole located at the center. The Debye screening length is ≈26 nm.

Simulation—We model the interactions between our dipolar active colloids by a hybrid potential that combines the short-range repulsive Weeks-Chandler-Anderson (WCA) potential with a dipole-dipole (DD) pair interaction [38]. In experiment, the dipole moments are aligned with the oscillating electric field $\mathbf{E} = E\hat{\mathbf{z}}$ [33,35]. Hence, all particles have a dipole moment $\mathbf{p} = p\hat{\mathbf{z}}$ with dipole strength p (that increases with $|E|$). The interaction potential between particles i and j, is $U_{HY,ij} = U_{\mathrm{WCA}}(r_{ij}) + U_{\mathrm{DD}}(\mathbf{p}, r_{ij})$ with

$$U_{\mathrm{WCA}}(r) = 4\epsilon\left[\left(\frac{\sigma}{r}\right)^{12} - \left(\frac{\sigma}{r}\right)^{6}\right], \quad r < 2^{1/6}\sigma,$$
$$U_{\mathrm{DD}}(\mathbf{p}, r) = \frac{1}{r^3}(\mathbf{p}\cdot\mathbf{p}) - \frac{3}{r^5}(\mathbf{p}\cdot\mathbf{r})(\mathbf{p}\cdot\mathbf{r}), \tag{1}$$

where $\mathbf{r}_{ij} = \mathbf{r}_i - \mathbf{r}_j$ is the interparticle separation and $r_{ij} = |\mathbf{r}_{ij}|$. We choose units such that the WCA potential strength $\epsilon = 1$ and the particle diameter is $\bar{\sigma} = 2^{1/6}\sigma = 1$. The DD pair interaction is attractive along the direction of the polarization $\mathbf{p}$ and repulsive in the orthogonal plane, naturally leading to the formation of parallel strings along $\hat{\mathbf{z}}$. Because of ICEP, each Janus particle rotates until the interface between the two halves is parallel to $\mathbf{E}$, and therefore self-propels in a direction in the xy plane [Fig. 1(d)]. The Debye screening length in experiment is much smaller than particle diameter, allowing us to cut off dipole interactions after the first neighbor for computational efficiency.

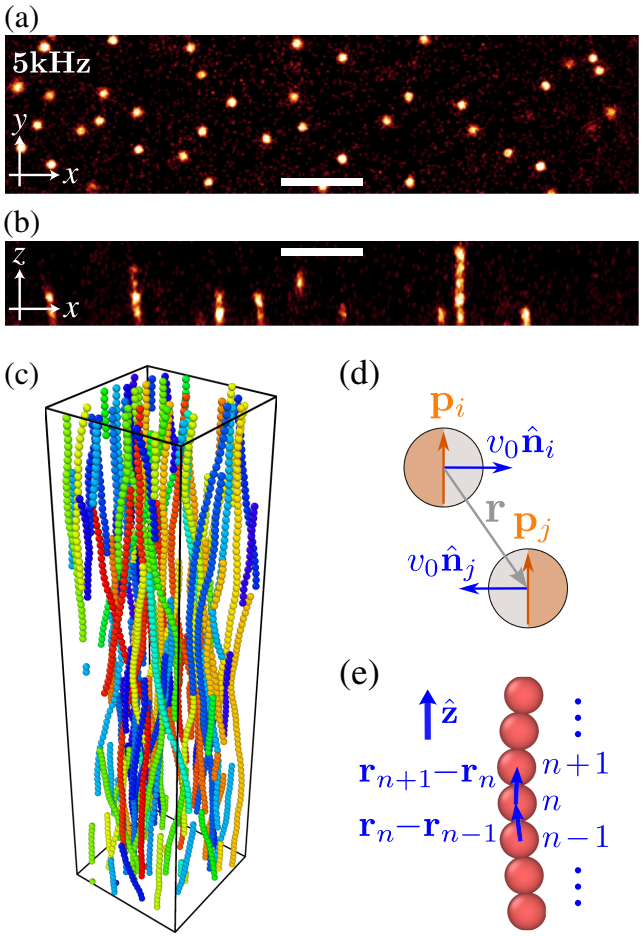

FIG. 1. The active travelling string system in experiment and simulation. (a),(b) Confocal microscopy images of the experimental system with electric field amplitude $E = \frac{1}{3}$ V/μm at 5 kHz frequency; in the lateral xy plane (a) and vertical xz plane (b). Scale bars are 10 μm. The experimental data (and SM movie 1 and snapshots) are samples taken far from the experimental boundaries in the x, y direction and the upper z boundary but close to the lower z boundary. (c) Snapshot from simulations visualized in OVITO [40], at packing fraction 5%: different colors indicate different clusters. (d) Schematic of the Janus particle used in experiments. The dipoles $\mathbf{p}_i = (0, 0, p)$ are aligned with electric field direction and perpendicular to self-propelling velocities $\mathbf{v}_0 = v_0(\cos\theta_i, \sin\theta_i, 0)$. $\mathbf{r} = (x, y, z)$ is the vector separating the positions of two bead centers. (e) The bond vector for a single string, with $\boldsymbol{r}_n$ the position of the nth bead.

We combine $U_{HY,ij}$ with overdamped active Brownian dynamics without hydrodynamics,

$$\dot{\mathbf{r}}_i = -\frac{1}{\zeta}\sum_{j\neq i}\boldsymbol{\nabla}_i U_{HY,ij} + v_0\hat{\mathbf{n}}_i + \boldsymbol{\eta}_i^T,$$
$$\hat{\mathbf{n}}_i = (\cos\theta_i, \sin\theta_i, 0), \quad \dot{\theta}_i = \eta_i^R, \tag{2}$$

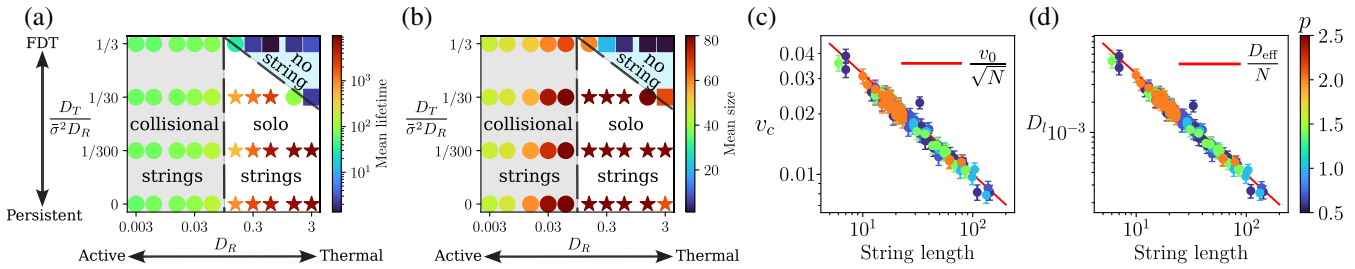

FIG. 2. (a),(b) Phase diagrams of the mean lifetime and mean size of traveling strings. $p = 1$, $v_0 = 0.5$ as a function of rotational diffusion coefficent D_R and ratio $(D_T/\bar{\sigma}^2 D_R)$. The three regimes and markers in these phase diagrams are determined by the mean lifetime phase diagram. The color bar in the mean size phase diagram is linear and is logarithmic in the mean lifetime phase diagram. These phase diagrams are based on simulations with periodic boundary box size $20 \times 20 \times 80$. (c) Self-propulsion speed of string centroids v_c. (d) Collective longtime diffusion coefficient D_l [see Eq. (4)]. The two red lines are our theoretical predictions Eq. (4). Data are extracted from simulations at $v_0 = 0.1$, $D_R = 0.15$, $(D_T/\bar{\sigma}^2 D_R) = (1/30)$, $p \in [0.6, 0.7, 1.0, 1.4, 2.0]$, with color bars indicating dipole strength p. Error bars correspond to the standard deviation of the data. The D_l data are obtained from v_c and the collective translational diffusion coefficient D_c [see Fig. S3.2 [43] and Eq. (4)]. v_c dominates D_l in this regime resulting in similar plot shapes. Error estimated by assuming independent normal distributions. All data are picked from the last 5000 time units in steady state.

where $\{\mathbf{r}_i, \theta_i\}$ are the position, orientation of the ith particle, and ζ is the Stokes drag. We include activity with self-propulsion speed v_0 (that in experiment increases with $|E|$) in the direction $\hat{\mathbf{n}}_i$, which is constrained to the xy plane, orthogonal to $\hat{z}$ [Fig. 1(d)]. Its in-plane angle θ_i diffuses with rotational white noise η_i^R, with correlation $\langle \eta_n^R(t)\eta_m^R(t')\rangle = 2D_R\delta(t-t')\delta_{nm}$, where D_R is the rotational diffusion coefficient. We also include translational white noise $\boldsymbol{\eta}_i^T$ in all directions, with correlations $\langle \eta_{\alpha n}^T(t)\eta_{\beta m}^T(t')\rangle = 2D_T\delta(t-t')\delta_{\alpha\beta}\delta_{nm}$ where D_T is the translational diffusion coefficient. For most runs, the simulation box is periodic in all three dimensions and we use LAMMPS [41] with a custom ABP integrator [42].

In our simulations, we systematically vary the dipole strength, speed, and diffusion coefficients via the parameters $[p, v_0, D_R, (D_T/\bar{\sigma}^2 D_R)]$ while maintaining a fixed low volume fraction $\phi = 0.05$. Strings are defined by a clustering algorithm with neighbor cutoff distance $1.05\bar{\sigma}$ [Fig. 1(c)]. Here, we first locate the transition to the string phase by varying p and v_0 independently for intermediate $D_R = 0.15$ and different D_T [Figs. S2.1(a)–S2.1(d) [43]]. The transition from a disordered phase at low p to a string phase at high p shifts from around $p = 0.2$–0.3 at $v_0 = 0.1$ to $p \lesssim 1$ at $v_0 = 0.7$. Then we fix $p = 1$ and $v_0 = 0.5$, which is in the string phase in almost all cases.

We find that string formation is subject to slow coarsening dynamics, necessitating runs of $t = 20\,000$ time units to reach steady state (Fig. S2.2a [43]). Strings also rapidly lengthen when p increases (Fig. S2.2b [43]), and we switch to a tall simulation box $L_x \times L_y \times L_z \equiv 20 \times 20 \times 80$ for our main runs [Fig. 1(c)]. Strings can still span the system, so we cut off string size at $L_z/\bar{\sigma} = 80$.

The persistence of active driving is regulated by rotational, D_R and translational, D_T diffusion. If fluctuation-dissipation theorem (FDT) holds, $D_T = k_B T/\zeta$ and $D_R = k_B T/\zeta_r$. For Stokes' drag, where $\bar{\sigma}^2\zeta = 3\zeta_r$ this implies that $(D_T/\bar{\sigma}^2 D_R) = \frac{1}{3}$ in simulation units. Another limit [27], is where orientational noise dominates and $D_T \approx 0$ ("persistent"). Finally, when D_R is very large we have an effectively thermal system with a renormalized *active* temperature ("thermal") [Supplemental Material (SM) movies 4–5 [43]]. The two axes of our phase diagrams are then D_R and $(D_T/\bar{\sigma}^2 D_R)$, with D_R varying from 0.003 to 3, which correspond to an active limit and a thermal limit respectively. $(D_T/\bar{\sigma}^2 D_R)$ varies from 0 to $\frac{1}{3}$, which indicate a persistent limit and the FDT limit, respectively. With this parameter scan, we construct a phase diagram that focuses on *active* string dynamics [Figs. 2(a) and 2(b)]. We measure the mean size and mean lifetime of strings, defined as time interval between changes in string composition. With the exception of a stringless phase at high D_R and D_T, i.e., a thermal FDT limit, the value of D_R predicts string properties. We find a phase of medium-sized strings that interact through *collisions* with lifetimes $\tau_l \sim 100$ when D_R is relatively low ($D_R \leq 0.06$) and a phase of noninteracting *solo* strings with rapidly increasing τ_l and lengths that exceed the system size and wrap the box when $D_R \geq 0.15$. *Collisional* strings move persistently and collide frequently (SM movies 2 and 3 [43]), while *solo* strings move diffusively with almost no collisions (SM movie 4; Sec. 2 of SM [43]).

We probe the collective motion of traveling strings, first focusing on the motion of their centroids. We can fit the mean square displacement (MSD) of the centroids of the strings in the xy plane to the MSD of an isolated two-dimensional (2D) ABP [44,45]. The collective longtime diffusion coefficient of centroids decays with string length as $D_l \sim N^{-1}$ [see Fig. 2(d) and Eq. (4)], whereas the collective self-propulsion speed decays with the square root of length $v_c \sim N^{-1/2}$ [Fig. 2(c)], and both are independent of dipole strength p, and phase.

Active anisotropic Rouse model—We can understand the string dynamics by mapping a single string to an active polymer model. Solving $\boldsymbol{\nabla} U_{HY}(\mathbf{r}) = 0$, gives the stable equilibrium separation between two particles $\boldsymbol{r}^{(0)} = (0, 0, \pm a(p))$, which depends on the dipole strength p. Expanding the hybrid potential U_{HY} near $\boldsymbol{r}^{(0)}$, gives an effective elastic potential $U_E := \frac{1}{2}(\mathbf{r} - \boldsymbol{r}^{(0)}) \cdot \mathbf{H}_U(\boldsymbol{r}^{(0)}) \cdot (\mathbf{r} - \boldsymbol{r}^{(0)})^T$. The Hessian matrix, $\mathbf{H}_U$, is diagonal with effective elastic constants, $\kappa_{11}(p) := (\partial^2 U_{HY}/\partial x^2)|_{\mathbf{r}=\boldsymbol{r}^{(0)}} = (\partial^2 U_{HY}/\partial y^2)|_{\mathbf{r}=\boldsymbol{r}^{(0)}}$ and $\kappa_{33}(p) := (\partial^2 U_{HY}/\partial z^2)|_{\mathbf{r}=\boldsymbol{r}^{(0)}}$, functions of p and isotropic in the xy plane. Both strongly increase with p, and $\kappa_{33} \gg \kappa_{11}$. See SM Sec. 3.1 for details [43].

For a string of size N, the position of the nth particle can be expanded around a rigid column as $\boldsymbol{r}_n := \boldsymbol{r}_n^{(0)} + \mathbf{R}_n$ where $\boldsymbol{r}_n^{(0)} = (0, 0, an)$ and fluctuations $\mathbf{R}_n = (R_{1n}, R_{2n}, R_{3n}) := (x_n, y_n, z_n)$, $1 \le n \le N$ [Fig. 1(e)]. The equations of motion for the strings therefore are an active anisotropic Rouse model [46] (see SM Sec. 3.2 [43]),

$$\dot{R}_{\alpha n} = \frac{\kappa_{\alpha\alpha}}{\zeta}\frac{\partial^2 R_{\alpha n}}{\partial n^2} + A_{\alpha n} + \eta^T_{\alpha n}, \qquad \dot{\theta}_n = \eta^R_n, \tag{3}$$

for $\alpha = 1, 2, 3$. Here, activity $\mathbf{A}_n = (A_{1n}, A_{2n}, A_{3n})$ is confined to the xy plane, i.e., $A_{1n} = v_0 \cos\theta_n$, $A_{2n} = v_0 \sin\theta_n$ and $A_{3n} = 0$. Using Rouse modes [23,46], the equations can be solved analytically and various collective quantities obtained. See SM Secs. 3.2–3.4 for details [43].

The motion of the centroid of the string is given by the lowest (0th) Rouse mode. We therefore compute the MSD of the string centroid in the xy plane to obtain $\mathrm{MSD}_{\mathrm{string}} = 4D_c t + 2v_c^2 D_R^{-1}[t + D_R^{-1}(e^{-D_R t} - 1)]$, with an effective translational diffusion coefficient D_c and the collective self-propulsion speed v_c. Comparing the collective $\mathrm{MSD}_{\mathrm{string}}$ with that of a single ABP [44,45], we find

$$v_c = \frac{v_0}{\sqrt{N}}, \qquad D_c = \frac{D_T}{N}, \qquad D_l = D_c + \frac{v_c^2}{2D_R} = \frac{D_{\mathrm{eff}}}{N}. \tag{4}$$

We also obtain D_l, the longtime diffusion coefficient of string centroids in terms of $D_{\mathrm{eff}} = D_T + v_0^2/(2D_R)$, the longtime diffusion coefficient of an isolated Janus colloid with both translational noise and active driving. Our result also shows that the persistence time of the strings D_R^{-1} is the same as that of a single particle. Hence, we find the collective dynamics of traveling strings is solely governed by their length and Eq. (4) accurately predicts the simulation results [red lines in Figs. 2(c) and 2(d)].

In addition to their persistent centroid motion, the fluctuations along the strings are also highly spatially correlated [Fig. 1(c) and SM movies 2 and 3 [43]]. These mesoscale spatial correlations emerge from the active driving coupling to the long wavelength elastic modes [14,15].

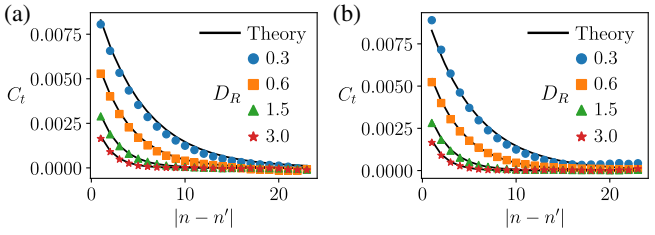

FIG. 3. Bond vector correlation functions in noninteracting (a) and interacting (b) string systems. Parameters are $p = 1$, $v_0 = 0.5$, $(D_T/\tilde{\sigma}^2 D_R) = (1/300)$. Points are simulation data, lines are theoretical predictions.

To illustrate this, we analyze the correlations of the *bond vectors*, i.e., $\boldsymbol{b}_n = \boldsymbol{r}_n - \boldsymbol{r}_{n-1}$, at different positions on the traveling strings [see Fig. 1(e)]. We find new active contributions which are due to the *finite time* correlations in the directions of local active driving. The relevant correlation function is the correlation between the *deviations* of the bonds from those of a rigid column: $\mathbf{B}_n = \mathbf{R}_n - \mathbf{R}_{n-1} = \boldsymbol{b}_n - (0, 0, a)$. We obtain an exact expression for this bond-vector deviation correlation function, $C_t(n, n') = \langle \mathbf{B}_n \cdot \mathbf{B}_{n'} \rangle$, using the higher Rouse modes (see SM Sec. 3.5 [43]): $C_t(n, n) = (2aD_a/\xi D_R)(e^{-(a/\xi)} - 1) + 2\zeta\{[(D_T + D_a)/\kappa_{11}] + (D_T/2\kappa_{33})\} := C_{t0}$ when $n = n'$, and

$$C_t(n, n') = \frac{aD_a}{\xi D_R}\left(e^{\frac{a}{\xi}} + e^{-\frac{a}{\xi}} - 2\right)e^{-\frac{a}{\xi}|n-n'|}, \tag{5}$$

which is valid when the bonds are far from the ends, $1 \ll n \ne n' \ll N$. Here, $D_a = (v_0^2/2D_R)$ is the active contribution to the ABP effective translational diffusion coefficient. The correlation length $\xi = a\sqrt{(\kappa_{11}/D_R\zeta)}$ of the exponential decay scales as the square root of active persistence time (Fig. S2.4a [43]). We note that in the thermal limit, the system is a flexible chain with no bond vector correlations when $n \ne n'$, i.e., the correlations are a purely active effect. Figure S2.4b shows how in the thermal limit $D_R \to \infty$, the $n = n'$ part of C_t decays to a constant proportional to D_T, whereas for $|n - n'| \ne 0$ it decays to 0. Equation (5) is an excellent match to simulations of an isolated (noninteracting) string system over several D_R [see Fig. 3(a)]. In the simulations we have subtracted the mean squared equilibrium distance between two consecutive particles, a^2 from $\langle \boldsymbol{b}_n \cdot \boldsymbol{b}_{n'} \rangle$. For interacting strings [see Fig. 3(b)], there is still excellent agreement if we modify the reference state for the bond deviations: $\mathbf{B}_n = \boldsymbol{b}_n - (0, 0, a_{em})$, with a_{em} determined by an empirical least squares fit. In Fig. S2.5, we show correlations for a range of D_R and the best fit a_{em}/a.

Here, we focus experiments with an external electric field amplitude $E = \frac{1}{3}$ V/μm at 5 kHz frequency, giving us

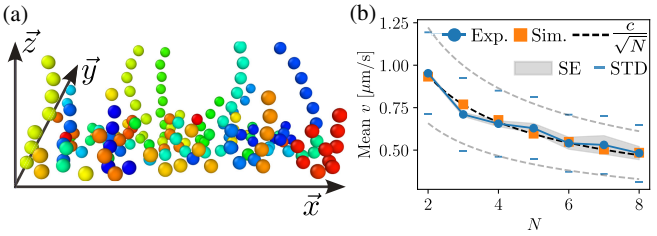

FIG. 4. (a) Coordinates from experimental data. Different colors indicate different strings. (b) Mean instantaneous speed plot. Dots are experiment data, squares are simulation data. We average the speed over strings of the same length. The best fit of the mean is $v = (c/\sqrt{N})$ [theory, Eq. (4)] with $c = 1.3$. The blue bars indicate the standard deviation (STD) and the shaded area is the standard error of the mean (SE) in experiment [49]. Simulation error bars are smaller than the square marker size.

an individual particle Péclet number $\mathrm{Pe} \approx 20$. Because of limited z resolution, we use TRACKPY [47] to first identify particles with good xy accuracy in individual z layers vertically spaced by $a_{\mathrm{eff}} = 2.6$ μm, the effective particle spacing at this salt concentration.

We find a landscape of cairnlike strings [48] (columns) with variable height growing from the bottom surface, due to the finite gravitational length [Fig. 4(a)]. To identify strings, we developed a clustering algorithm that follows strings from the top to the bottom by connecting to the nearest point, if any, within a_{eff}. Because of the finite scan time for each z layer, moving from the bottom to the top of the image *and* the fact that the strings are self-propelled, moving with instantaneous velocity $\mathbf{v}$ in the xy plane, the observed strings appear tilted. If the scan time of the string τ_s is less than D_R^{-1}, the string approximately travels in a fixed direction during the scan (we estimate $\tau_s \lesssim D_R^{-1}$). We can then measure the velocity $\mathbf{v}$ of traveling strings from the tilt angle (and plane) of the strings. We perform a least-squares analysis on the beads in the string to obtain a best fit straight line, l_s making an angle θ_s with $\hat{\mathbf{z}} = (0, 0, 1)$. $(\theta_s < (\pi/2))$. If in a time τ_s, the camera has scanned up to height z_s, then the string angle θ_s and its instantaneous speed $v = |\mathbf{v}|$ are related by $v\tau_s = \tan\theta_s z_s$. Using our imaging parameters, we find $v = 1.5802 \tan\theta_s$ μms^{-1} in our experiment. By averaging v over strings with the same length N we find that the mean v decays with N as $(1/\sqrt{N})$ [Fig. 4(b)], which is consistent with our simulations (performed near a bottom wall) and theory.

In conclusion, we have studied a string forming 3D active dipolar colloidal system using simulations, theory, and experiment. The collective dynamics of traveling strings, derived analytically and confirmed by numerical simulations and experimental analyses, has a simple dependence on string length. At low volume fractions, the string dynamics is well described by an active anisotropic Rouse model, showing emergent active bond vector correlations. In future work we plan to extend our analysis to the active sheets and labyrinth appearing at higher volume fractions [35], where we also expect additional hydrodynamic contributions to the dynamics.

Acknowledgments—The authors would like to thank the Isaac Newton Institute for Mathematical Sciences, Cambridge, for support and hospitality during the programme *New statistical physics in living matter*, where part of this work was done. This work was supported by EPSRC Grants No. EP/R014604/1 and No. EP/T031077/1. X. C. is supported by CSC-UoB (Bristol) joint Ph.D. Scholarship No. 202108060089. C. P. R. would like to acknowledge the Agence National de Recherche for the provision of the grant DiViNew.

[1] J. R. Baylis, J. H. Yeon, M. H. Thomson, A. Kazerooni, X. Wang, A. E. St. John, E. B. Lim, D. Chien, A. Lee, J. Q. Zhang *et al.*, Sci. Adv. **1**, e1500379 (2015).
[2] R. Di Leonardo, L. Angelani, D. Dell'Arciprete, G. Ruocco, V. Iebba, S. Schippa, M. P. Conte, F. Mecarini, F. De Angelis, and E. Di Fabrizio, Proc. Natl. Acad. Sci. U.S.A. **107**, 9541 (2010).
[3] S. Krishnamurthy, S. Ghosh, D. Chatterji, R. Ganapathy, and A. Sood, Nat. Phys. **12**, 1134 (2016).
[4] J. Stenhammar, R. Wittkowski, D. Marenduzzo, and M. E. Cates, Sci. Adv. **2**, e1501850 (2016).
[5] G. Frangipane, D. Dell'Arciprete, S. Petracchini, C. Maggi, F. Saglimbeni, S. Bianchi, G. Vizsnyiczai, M. L. Bernardini, and R. Di Leonardo, eLife **7**, e36608 (2018).
[6] J. Arlt, V. A. Martinez, A. Dawson, T. Pilizota, and W. C. Poon, Nat. Commun. **9**, 768 (2018).
[7] Y. Chen, X. Li, C. Scheibner, V. Vitelli, and G. Huang, Nat. Commun. **12**, 5935 (2021).
[8] M. C. Marchetti, J.-F. Joanny, S. Ramaswamy, T. B. Liverpool, J. Prost, M. Rao, and R. A. Simha, Rev. Mod. Phys. **85**, 1143 (2013).
[9] D. Humphrey, C. Duggan, D. Saha, D. Smith, and J. Käs, Nature (London) **416**, 413 (2002).
[10] T. Liverpool, A. Maggs, and A. Ajdari, Phys. Rev. Lett. **86**, 4171 (2001).
[11] T. Eisenstecken, G. Gompper, and R. G. Winkler, Polymers **8**, 304 (2016).
[12] B. Chakrabarti, Y. Liu, J. LaGrone, R. Cortez, L. Fauci, O. Du Roure, D. Saintillan, and A. Lindner, Nat. Phys. **16**, 689 (2020).
[13] S. C. Al-Izzi, P. Sens, M. S. Turner, and S. Komura, Soft Matter **16**, 9319 (2020).
[14] S. Henkes, K. Kostanjevec, J. M. Collinson, R. Sknepnek, and E. Bertin, Nat. Commun. **11**, 1405 (2020).
[15] L. Caprini, U. M. B. Marconi, and A. Puglisi, Phys. Rev. Lett. **124**, 078001 (2020).
[16] T. H. Tan, A. Mietke, J. Li, Y. Chen, H. Higinbotham, P. J. Foster, S. Gokhale, J. Dunkel, and N. Fakhri, Nature (London) **607**, 287 (2022).
[17] C. Scheibner, A. Souslov, D. Banerjee, P. Surówka, W. T. Irvine, and V. Vitelli, Nat. Phys. **16**, 475 (2020).
[18] V. Schaller, C. Weber, C. Semmrich, E. Frey, and A. R. Bausch, Nature (London) **467**, 73 (2010).

[19] A. Deblais, K. Prathyusha, R. Sinaasappel, H. Tuazon, I. Tiwari, V. P. Patil, and M. S. Bhamla, Soft Matter **19**, 7057 (2023).
[20] M. Fazelzadeh, E. Irani, Z. Mokhtari, and S. Jabbari-Farouji, Phys. Rev. E **108**, 024606 (2023).
[21] M. Kelidou, M. Fazelzadeh, B. Parage, M. van Dijk, T. Hooijschuur, and S. Jabbari-Farouji, J. Chem. Phys. **161**, 104904 (2024).
[22] D. Mizuno, C. Tardin, C. F. Schmidt, and F. C. MacKintosh, Science **315**, 370 (2007).
[23] T. Liverpool, Phys. Rev. E **67**, 031909 (2003).
[24] R. E. Isele-Holder, J. Elgeti, and G. Gompper, Soft Matter **11**, 7181 (2015).
[25] K. Prathyusha, S. Henkes, and R. Sknepnek, Phys. Rev. E **97**, 022606 (2018).
[26] S. Mandal, C. Kurzthaler, T. Franosch, and H. Löwen, Phys. Rev. Lett. **125**, 138002 (2020).
[27] M. C. Marchetti, Y. Fily, S. Henkes, A. Patch, and D. Yllanes, Curr. Opin. Colloid Interface Sci. **21**, 34 (2016).
[28] C. Bechinger, R. Di Leonardo, H. Löwen, C. Reichhardt, G. Volpe, and G. Volpe, Rev. Mod. Phys. **88**, 045006 (2016).
[29] M. E. Cates and J. Tailleur, Annu. Rev. Condens. Matter Phys. **6**, 219 (2015).
[30] T. M. Squires and M. Z. Bazant, J. Fluid Mech. **560**, 65 (2006).
[31] S. Gangwal, O. J. Cayre, M. Z. Bazant, and O. D. Velev, Phys. Rev. Lett. **100**, 058302 (2008).
[32] A. E. Patteson, A. Gopinath, and P. E. Arratia, Curr. Opin. Colloid Interface Sci. **21**, 86 (2016).
[33] J. Yan, M. Han, J. Zhang, C. Xu, E. Luijten, and S. Granick, Nat. Mater. **15**, 1095 (2016).
[34] J. Zhang, R. Alert, J. Yan, N. S. Wingreen, and S. Granick, Nat. Phys. **17**, 961 (2021).
[35] N. Sakaï and C. P. Royall, arXiv:2010.03925.
[36] R. Tao, J. Phys. Condens. Matter **13**, R979 (2001).
[37] A. Yethiraj and A. Van Blaaderen, Nature (London) **421**, 513 (2003).
[38] A.-P. Hynninen and M. Dijkstra, Phys. Rev. Lett. **94**, 138303 (2005).
[39] A. Ivlev, G. Morfill, H. Lowen, and C. P. Royall, *Complex Plasmas and Colloidal Dispersions: Particle-Resolved Studies of Classical Liquids and Solids* (World Scientific Publishing Company, Singapore, 2012), Vol. 5.
[40] A. Stukowski, Model. Simul. Mater. Sci. Eng. **18**, 015012 (2009).
[41] A. P. Thompson, H. M. Aktulga, R. Berger, D. S. Bolintineanu, W. M. Brown, P. S. Crozier, P. J. In't Veld, A. Kohlmeyer, S. G. Moore, T. D. Nguyen *et al.*, Comput. Phys. Commun. **271**, 108171 (2022).
[42] S. Cameron, M. Mosayebi, R. Bennett, and T. B. Liverpool, Phys. Rev. E **108**, 014608 (2023).
[43] See Supplemental Material at http://link.aps.org/supplemental/10.1103/PhysRevLett.134.018302 for more details.
[44] J. R. Howse, R. A. Jones, A. J. Ryan, T. Gough, R. Vafabakhsh, and R. Golestanian, Phys. Rev. Lett. **99**, 048102 (2007).
[45] D. Breoni, M. Schmiedeberg, and H. Löwen, Phys. Rev. E **102**, 062604 (2020).
[46] M. Doi and S. F. Edwards, *The Theory of Polymer Dynamics* (Oxford University Press, New York, 1988), Vol. 73.
[47] D. B. Allan, T. A. Caswell, N. C. Keim, and T. contributors, Trackpy: Trackpy v0.6.4 (2024), 10.5281/zenodo.1213240.
[48] Https://en.wikipedia.org/wiki/Cairn
[49] J. R. Taylor, *An Introduction to Error Analysis: The Study of Uncertainties in Physical Measurements* (University Science Books, Sausalito, 1997).